Parsing the roles of neck-linker docking and tethered head diffusion in the stepping dynamics of kinesin

Zhechun Zhang[a], Yonathan Goldtzvik[a,b], and D. Thirumalai[b,1]

[a]Biophysics Program, Institute for Physical Science and Technology, University of Maryland, College Park, MD 20742; and [b]Department of Chemistry, University of Texas at Austin, Austin, TX 78712

Edited by José N. Onuchic, Rice University, Houston, TX, and approved October 3, 2017 (received for review April 11, 2017)

Kinesin walks processively on microtubules (MTs) in an asymmetric hand-over-hand manner consuming one ATP molecule per 16-nm step. The individual contributions due to docking of the approximately 13-residue neck linker to the leading head (deemed to be the power stroke) and diffusion of the trailing head (TH) that contributes in propelling the motor by 16 nm have not been quantified. We use molecular simulations by creating a coarse-grained model of the MT–kinesin complex, which reproduces the measured stall force as well as the force required to dislodge the motor head from the MT, to show that nearly three-quarters of the step occurs by bidirectional stochastic motion of the TH. However, docking of the neck linker to the leading head constrains the extent of diffusion and minimizes the probability that kinesin takes side steps, implying that both the events are necessary in the motility of kinesin and for the maintenance of processivity. Surprisingly, we find that during a single step, the TH stochastically hops multiple times between the geometrically accessible neighboring sites on the MT before forming a stable interaction with the target binding site with correct orientation between the motor head and the α/β tubulin dimer.

bidirectional stochasticity | microtubule-kinesin complex | tethered head diffusion | minimizing side steps | power stroke

Directional transport of intracellular vesicles along polar tracks [actin and microtubule (MT)] is carried out by a variety of molecular motors (1). The crucial function is executed by the three families of motor proteins (myosin, kinesin, and dynein), many of which preferentially move toward a certain direction along a particular polar cytoskeletal track (2). For example, kinesin-1 (Kin1) or conventional kinesin, pulls cargo toward the plus (+) end of the MT (2–4). It is now firmly established, thanks to a number of high-precision experiments, that kinesin with two motor domains walks in a hand-over-hand manner (5–8), by consuming one ATP molecule per step (9). Despite the small size of the motor domain, Kin1 is a powerful and fast motor, moving toward the (+) end of the MT, resisting forces up to 7 pN (10, 11), which is larger than or equal to the stall forces of bigger motors (12, 13), such as dynein (1–7 pN) and myosin (∼3 pN). Kin1 moves toward the (+) end processively at a speed of ∼800 nm/s (10), which is greater than both myosin V (∼400 nm/s) and dynein (∼100 nm/s) (14).

A remarkable series of experimental studies (3, 6, 15–17) from a number of groups has revealed many of the details of the stepping mechanism of kinesin. Two mechanisms have been proposed to explain how kinesin converts chemical energy to mechanical work to walk toward the (+) end of the MT in a hand-over-hand manner. According to the "power stroke" model (8), neck linker (NL) docking induced by ATP binding to the MT-bound leading head (LH) pulls the trailing head (TH) into the neighborhood of the target binding site (TBS) that is 16 nm away from the initial binding site (IBS). In this model, the NL with ∼13 residues connecting the motor domain to the coiled coil may be structurally analogous to the easily identifiable lever arm in myosin motors (2). In contrast, the "Brownian ratchet" model (18) posits that ATP hydrolysis in the TH allows it to detach from the MT to initiate biased diffusional search toward the TBS.

Both models have experimental support. Experiments using single-molecule FRET (fluorescence resonance energy transfer) (19) and fluorescence anisotropy (20) show that the NL docks (power stroke) upon ATP binding to the LH, raising the possibility that the motility of kinesin arises predominately from the power stroke mechanism. An optical trap experiment (21) shows that a kinesin mutant, which lacks the cover strand (a major docking site of the NL), can still walk processively, but generates much less force. It can, therefore, be concluded that NL docking must contribute significantly to force generation. In all likelihood, both power stroke and diffusion are operative in the stepping of kinesin. Until recently (22), the extent of diffusive motion of kinesin had not been reported in experiments (3), although a number of observations support the importance of the Brownian ratchet model. First, the small size of even a fully stretched NL limits the potential physical displacement of the TH upon NL docking to the LH (3). Second, the temperature dependence of the stepping rates indicates an entropic nature of directional bias (18) that cannot be explained solely by the NL docking model. However, the observation that the mutant lacking cover strand walks processively indicates that kinesin could walk by a Brownian ratchet mechanism in the absence of external load.

The two mechanisms are not mutually exclusive (3, 23, 24). Therefore, an unresolved question is: What fraction of the kinesin step is associated with power stroke and diffusion, respectively (3, 25)? If a large fraction of the step is associated with power stroke, we expect the TH to move almost unidirectionally covering a majority of the 16 nm, and the bidirectional diffusion

Significance

Like all motors, the stepping of the two-headed conventional kinesin on the microtubule (MT) is facilitated by conformational changes in the motor domain upon ATP binding and hydrolysis. Numerous experiments have revealed that docking of the 13-residue neck linker (NL) to the motor domain of the leading head plays a critical role in propelling the trailing head toward the plus end of the microtubule by nearly 16 nm in a single step. Surprisingly, our molecular simulations reveal that nearly three-quarters of the step occur by stochastic diffusion of the trailing head. Docking of the NL restricts the extent of diffusion, thus forcing the motor to walk with overwhelming probability on a single protofilament of the MT.

Author contributions: Z.Z. and D.T. designed research; Z.Z., Y.G., and D.T. performed research; D.T. contributed new reagents/analytic tools; Z.Z., Y.G., and D.T. analyzed data; and Z.Z., Y.G., and D.T. wrote the paper.

The authors declare no conflict of interest.

This article is a PNAS Direct Submission.

[1]To whom correspondence should be addressed. Email: dave.thirumalai@gmail.com.

This article contains supporting information online at www.pnas.org/lookup/suppl/doi:10.1073/pnas.1706014114/-/DCSupplemental.

could occur only within the neighborhood of the TBS. On the other hand, if a majority of the 16-nm step is covered by diffusion of the TH, we expect the motion of the TH to be bidirectional, and the extent of stochastic random walk of the TH to be large (>8 nm, half of the step size). However, if the kinesin step is largely diffusive, what keeps the motor on a single protofilament of the MT (26–28), which contains multiple protofilaments?

To distinguish between the predictions of these two (extreme) models, the motion of the kinesin motor head has to be tracked at a microsecond temporal resolution. Despite spectacular advances in using microscopy methods (see, for example, ref. 22) to visualize the stepping kinetics of motors, the needed time resolution to unambiguously track the position of the stepping motor has not been reached. Numerous experiments, starting with the pioneering study by Block and coworkers (29), which map the motion of the kinesin head (or the position of the load) at lower temporal resolution, show an apparently unidirectional step between the IBS (0 nm) and the TBS (16 nm). The mechanism of TH motion is "hidden" in the jump time (∼30 μs) between the waiting state, detachment of the TH, and subsequent attachment to the MT (both heads are bound to the MT) of kinesin. Unless experiments can track the molecular events in the motor head on shorter time scales (∼5–10 μs), one cannot unambiguously assess the interplay of power stroke (involving a structural change in the NL) and stochastic motion of the tethered head in resolving the 8-nm step of kinesin.

Given that a globular protein of the size of kinesin head with radius of gyration $R_g \approx 2$ nm can diffuse 16 nm within $\tau \sim \frac{(16nm)^2}{2D} \sim \frac{(16nm)^2}{2\frac{k_B T}{6\pi\eta R_g}} \sim 4$ μs in a medium as viscous as cytoplasm, microsecond resolution may be needed to capture the potential importance of the stochastic bidirectional motion of the TH. However, due to difficulties in tracking kinesin experimentally at microsecond resolution (3), the importance of diffusivity of the kinesin step has been stressed (3, 18) but has not been quantified.

Here, we use Brownian dynamics of a coarse-grained (CG) model of the MT–kinesin (MT–Kin) complex to monitor the motion of kinesin during the 16-nm step at high temporal resolution (24). Such models (30) have provided considerable insights into a variety of complex biological systems, as first illustrated by Hyeon and Onuchic (HO) (23) in the context of stepping of kinesin. Our simulations, which produce a physically realistic picture of how kinesin steps on MT, allow us to follow the motion of the TH and the NL of the LH separately at submicrosecond resolution by generating several hundred trajectories. We show that a substantial portion of the kinesin step occurs by a diffusive process. However, NL docking provides severe restrictions on the conformational space explored by the TH during the stochastic search for the TBS. Thus, a combination of NL docking and a diffusive search for the TBS (16 nm away) is needed for executing the movement of the TH predominantly toward the (+) end of the MT in the absence of an external resistive force.

Results

Our model, which mimics the typical single-molecule experimental setup closely, consists of the two heads bound to the MT in the resting state. Following our previous study (24), we include three MT protofilaments, two motor heads, a coiled coil (length ≈ 30 nm) and a spherical cargo with 500-nm radius. The coiled coil is connected to the junction at which the two NLs, one from each motor domain, meet. The spherical cargo is attached to the ends of the coiled coil. To probe the possibility that the detached motor head could explore the binding sites on the neighboring protofilaments, we create a model (details in *SI Appendix*) containing 3 of the 13 MT protofilaments.

Two Energy Scales Determine Kinesin Motility. To ensure that the simulations are realistic, we first reproduce two important experimentally measured mechanical properties of the kinesin motor, the stall force (F_s) (10, 11) and the force required to unbind TH from the MT (F_u) (31). We expect that F_s and F_u should depend on the two energy scales ϵ_h^{LH-NL} (the interaction strength between the NL and the LH) and ϵ_h^{TH-MT} (the interaction between the TH and the MT) (24). Determination of the range of ϵ_h^{LH-NL} values that reproduces the measured F_s is needed for a realistic description of the NL–LH interaction, which largely determines the role of power stroke in facilitating the kinesin step. Furthermore, the model has to reproduce the measured value of F_u that depends on realistic modeling of the TH–MT interaction, which, in turn, affects not only the probability that Kin1 could take side steps, but also determines the final stages of motor head–MT recognition (24). The two energy scales, needed to reproduce F_s and F_u, are independent. Residues participating in the LH–NL interaction are in the LH. In contrast, residues essential for TH–MT interaction are in the TH. In addition, our previous study (24) demonstrated that ϵ_h^{LH-NL} and ϵ_h^{TH-MT} affect different stages of kinesin step.

Determination of ϵ_h^{LH-NL}. For each ϵ_h^{LH-NL}, we first perform a set of control simulations in which no external force is applied to kinesin (*SI Appendix*, Fig. S1*B*) and then another set of simulations in the presence of a resistive force of 7 pN (*SI Appendix*, Fig. S1 *A* and *B*). For each set, we measure the probability (P_f) that TH steps forward to the TBS, as well as the probability (P_b) that TH goes back to the IBS. Optical trap experiments (10, 11) indicate that, $P_f = P_b$ at the stall force, $F_s = 7$ pN. Our simulations show that only for a narrow range of ϵ_h^{LH-NL}, $P_f \approx P_b$ at $F_s = 7$ pN. At F_s, with $\epsilon_h^{LH-NL} = 0.3$ kcal/mol, we find that $P_f \approx P_b$ (*SI Appendix*, Fig. S1 *B* and *C*). In a control simulation with $F = 0$, kinesin predominately moves forward (*SI Appendix*, Fig. S1 *B* and *C*). In the rest of this work, we set $\epsilon_h^{LH-NL} =$ 0.3 kcal/mol.

Calibrating the MT–TH Interaction by Reproducing the Unbinding Force (F_u). Experiments show that the unbinding force for monomeric kinesin varies from 3 to 9 pN depending on the nucleotide condition (31). To obtain ϵ_h^{TH-MT}, we perform simulations by initially binding a single motor head to the MT (*SI Appendix*, Fig. S1*D*), just like in the experimental setup, to obtain F_u. By performing hundreds of simulations using various combination of ϵ_h^{TH-MT} and F, we are able to find the values of ϵ_h^{TH-MT} that allow kinesin to bind stably to the MT in the absence of F (*SI Appendix*, Fig. S1 *E* and *F*), but detaches at 3 pN corresponding to the weakly bound state (*SI Appendix*, Fig. S1*E*) or 9 pN corresponding to the strongly bound state (*SI Appendix*, Fig. S1*F*). Therefore, by varying ϵ_h^{TH-MT}, we can mimic both the weak and strong binding states that kinesin experiences during the reaction cycle. Because the exact timing and condition for ADP release, which strengthens the MT–Kin interaction, is still unknown, here we perform simulations under conditions that mimic both weak and strong binding.

Translation Motion of the TH Is Diffusive. A key finding in our simulations is that the search for the TBS is a predominately diffusive process, independent of our choice of ϵ_h^{TH-MT}. We observe large-scale bidirectional diffusive motion of the TH throughout the 16-nm step. For example, four representative trajectories where TH completes the 16-nm step (Fig. 1 *A*–*D*), with varying first passage times, show that the center of mass of the TH fluctuates extensively (along the MT axis). The duration of such bidirectional diffusional search varies from $<$ 10 μs (Fig. 1*A*) to $>$ 100 μs (Fig. 1*D*).

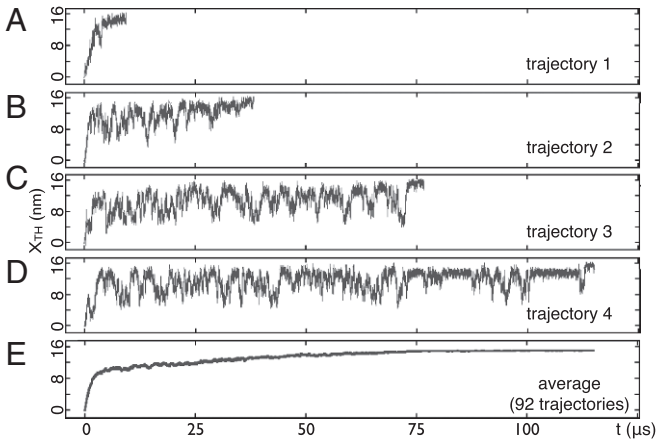

Fig. 1. Diffusive nature of the kinesin step. (*A–D*) Translational motion of (the center of mass) of the TH along the MT axis in four trajectories of the 16-nm step of kinesin, quantified by using the time-dependent changes of the center of mass of the TH, x_{TH}, along the MT axis. (*E*) Ensemble average of x_{TH} based on 92 trajectories. The average can be best fit by using $x_{TH}(t) = 15.7 - 8.5e^{(-t/1.1\,\mu s)} - 6.4e^{(-t/40.1\,\mu s)}$, where the coefficient are in units of nanometers. Note that at $t = 0$, $x_{TH}(t = 0) = 0.9$ nm, which is roughly the equilibrium value of x_{TH}. At long times $x_{TH} = 15.7$ nm. Thus, $x_{TH}(t)$ increases from $t = 0$ until stepping is completed.

The ensemble average of $x_{TH}(t)$ (Fig. 1*E*) also shows that the TH spends a considerable amount of time undergoing stochastic motion, even as it is poised to reach the TBS. The average motion of the TH (along the MT axis, based on 92 trajectories) shows a fast and a slow phase. The fast phase, occurring within 1.1 μs, corresponds to the relaxation of the TH after detachment from the MT and the forward motion induced by NL docking in the LH. The slow phase, with an average time constant of 40.2 μs, corresponds to the diffusional search for the TBS. We find that the fast and slow phases are robust to choice of ϵ_h^{TH-MT} (*SI Appendix*, Fig. S3). The time constant for the slow phase does not significantly depend on ϵ_h^{TH-MT}, as long as its value is in a range for stable binding of the TH to the MT. However, if ϵ_h^{TH-MT} is too weak, the TH could spontaneously detach due to thermal fluctuation, and motor processivity would be lost. As ϵ_h^{TH-MT} decreases, the time constant corresponding to the slow phase could exceed 40.2 μs, an estimate based on a value of ϵ_h^{TH-MT} that reproduces the experimental unbinding force of 6–9 pN. From the additional simulations and the arguments given above, we conclude that for physically reasonable values of ϵ_h^{TH-MT}, the time constants are not greatly affected, allowing us to conclude strongly that temporally >95% of the kinesin step is associated with diffusion.

A close examination of a typical trajectory (Fig. 2) reveals that diffusion starts immediately after the TH detaches from the MT. Even when x_{TH} reaches 10 nm at ∼1 μs, it subsequently decreases to ∼3 nm (Fig. 2*E*). At a later time, the TH enters the neighborhood of the TBS at $t \sim 17$ μs (Fig. 2*B* and arrow in Fig. 2*F*), but again retreats to a position behind the MT-bound LH at ∼20 μs (Fig. 2*E*). Additional evidence for diffusion outside the neighborhood of the TBS comes from the recording of d_{TH}, the distance between the TH and the TBS, as a function of time (Fig. 2 *C* and *F*). It is also clear from Fig. 2*F* that the TH stochastically searches for the TBS upon detachment from the MT. The diffusive characteristics of the trajectory depicted in Fig. 2 is typical, and we find similar behavior in all of the other stepping trajectories as well (for example, the ones illustrated in Fig. 1). We surmise from the time-dependent changes in both x_{TH} and d_{TH} that the TH undergoes bidirectional diffusion not only within the neighborhood of the TBS, but also throughout the 16-nm step.

TH Undergoes Isotropic Rotational Diffusion. Time-dependent changes in x_{TH} and d_{TH} reveal only one facet of diffusive behavior of the TH during the kinesin step. The TH also undergoes rotational diffusion. We use θ_{TH} (Fig. 2*B*) to quantify the extent of rotation of the TH with respect to its center of mass. At $t = 0$, $\theta_{TH} \approx 0°$ (Fig. 2*G*), implying that the TH is bound to the MT with the same orientation as observed in cryo-EM image of the MT–Kin complex ($\vec{e}_0$ in Fig. 2*A*). We assume that stepping is complete only after the TH achieves the same orientation in the TBS ($\theta_{TH} \approx 0°$). During the stepping process, θ_{TH} changes randomly between 0° and 180° (Fig. 2*G*). In the representative trajectory shown in Fig. 2, the TH is in the vicinity of the TBS at ∼17.5 μs. However, at this instant, the value of θ_{TH} is close to 70° (Fig. 2*G*), which implies that one of the principal axes of the TH that is initially parallel to the MT axis when the TH is bound to the MT (black arrow in Fig. 2*A*) is almost perpendicular to the MT axis (black arrow in Fig. 2*B*). Because of the incorrect orientation, the TH fails to bind to the TBS at 17 μs and diffuses away from the TBS. Only at $t \sim 26$ μs does the TH achieve the correct orientation (∼ 0°; Fig. 2*D*).

The rotational motion of the TH is as important as translation, because kinesin head cannot bind to the MT and function with incorrect orientation ($\theta_{TH} \neq 0$). It has been shown, by using alanine scanning, that all residues responsible for MT binding are located on one side of kinesin (32). Furthermore, crystal structures of the intermediate states during Mg·ADP release and cryo-EM structure of the MT–Kin complex suggest that activation of kinesin requires multiple specific contacts with the MT (33). These results imply that stable binding between the TH and MT, as well as the function of kinesin, requires specific orientation between the motor head and the MT.

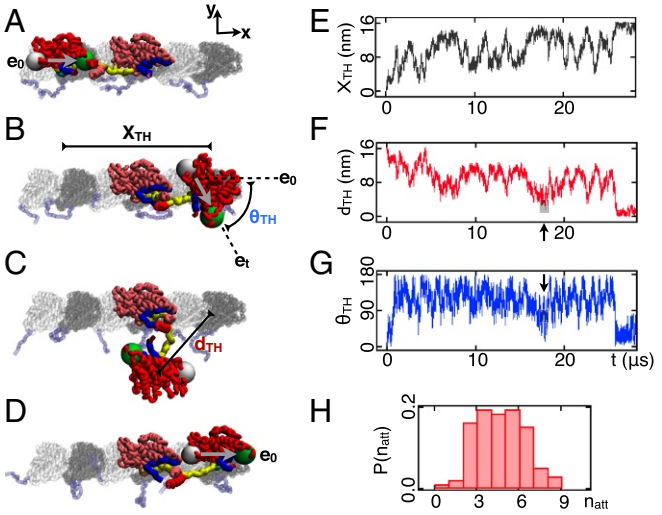

Fig. 2. Stochasticity in a 16-nm step of kinesin. (*A–D*) Four snapshots (at 0.0, 17.1, 19.3, and 27.8 μs) in a representative trajectory of the 16-nm step of kinesin. The TH is in red, and the LH is shown in pink. The yellow structure is the NL, and the docking site for the NL is in blue. α and β-tubulin are in silver and gray, respectively, and are augmented by ehooks (light blue). The black arrows ($\vec{e}_t$) indicates the orientation of the TH during the step, where $\vec{e}_t$ is an unit vector pointing from residue V40 to residue N221 of the TH. (*E*) Record of the translational motion of x_{TH}, the center of mass of the TH, along the MT axis during the 16-nm step. (*F*) The dependence of d_{TH}, the distance between the TH and the TBS as a function of *t*, in a representative trajectory. One unsuccessful attempt TH made to bind to the TBS is highlighted by the black arrow. (*G*) Time-dependent changes in the rotational motion, quantified by using $\theta_{TH}(t)$, of the TH (with respect to its center of mass) during the same 16-nm step as *B*. (*H*) Distribution of n_{att}, the number of times the TH reaches the TBS with incorrect orientation (the number of unsuccessful attempts), based on 92 trajectories.

To further demonstrate the importance of rotational diffusion of the TH, we calculate n_{att}, the number of times the TH retreats from the TBS due to incorrect orientation (Fig. 2*H*). In the trajectory shown in Fig. 2*G*, d_{TH} transiently reaches ∼0 nm at ∼ 17 μs. However, it remains unbound, at $t \sim 20$ μs because $\theta_{TH} \neq 0$. The distribution of the number of such failed attempts (Fig. 2*H*), based on 92 trajectories, shows that only in <5% of trajectories, the TH binds to the TBS with the correct orientation at the instant when $d_{TH} \approx 0$. Typically, the TH lands and unbinds ∼3–6 times before it can finish the 16-nm step that satisfies both the distance ($d_{TH} \approx 0$) and orientational ($\theta_{TH} \sim 0°$) criteria. This explains why in many trajectories the 16-nm step takes >30 μs to complete, even though the first passage times estimated based on translational diffusion coefficient and rotational diffusion coefficient (*SI Appendix*, Fig. S4) are only 3.0 and 4.0 μs, respectively. In other words, the first passage time is not the actual binding time (34). We note here in passing that neither the translational nor the rotational diffusion depends strongly on ϵ_h^{TH-MT} (*SI Appendix*, Fig. S4). Our simulations show that a great deal of stochasticity is involved in achieving an interface between the TH and MT that satisfies both the distance and orientation criteria.

Because of the diffusive nature of the motion, once the TH leaves the TBS, it could take the TH >10 μs to return to the TBS (between 17 and 25 μs in Fig. 2*G*, for example). During this time interval, the TH may diffuse as far as 10–12 nm away from the TBS, as illustrated in the time-dependent change in $d(t)$ after 17 μs in Fig. 2*G*. Together, our results show that search for the TBS involves both translational and rotational diffusion. Rotational diffusion of the TH is isotropic, but the anisotropic translation motion is greatly (in the absence of applied resistive force) biased toward the (+) end of the MT (24), which, we show below, is achieved by the NL docking to the LH.

A Large Diffusion Length Quantifies Stochasticity. Our simulations allow us to quantify the fraction of the kinesin step associated with the power stroke and that due to tethered diffusion. Although such a quantification has been reported for myosin motors (35) in experiments, a similar parsing of the kinesin step is undocumented. We use hundreds of trajectories to measure the fraction associated with power stroke and diffusion. For each trajectory, we first identify the instant when the power stroke associates with NL docking is complete (Fig. 3*A*, *Inset*). We calculate the diffusion length, x_{df}, by measuring the upper and lower values of x_{TH} that are reached after the completion of NL docking. For the trajectory in Fig. 3*A*, x_{TH} fluctuates between 4 and 16 nm after NL docks, and therefore $x_{df} = 12$ nm. The reason x_{TH} does not fluctuate between 0 and 16 nm is that once NL docks to the LH, the limited length of the stretched TH NL prevents the TH from diffusing back to the IBS. Thus, the lower bound, 4 nm, corresponds to the fraction of 16 nm due to power stroke (x_{ps}) in this trajectory. The distribution of x_{ps}, based on 100 trajectories, shows that, in general, the power stroke is responsible for 3–5 nm of the total 16-nm step (Fig. 3*A*). Therefore, the diffusion length has to be in the range ∼11–13 nm in most of the trajectories for successful completion of a step.

Kinesin Hops Stochastically Between Multiple Geometrically Accessible Binding Sites on the MT. Does TH visit binding sites on neighboring protofilaments? This question is pertinent not only because the MT has multiple protofilaments, but also because of our finding that nearly three-quarters of the 16-nm step is associated with diffusion of the TH. We find that the TH not only visits neighboring protofilaments, but also hops repeatedly between the binding sites on neighboring protofilaments and the TBS. For example, in a single trajectory (Fig. 3*B*, *Inset*), the TH first hops from the lower right binding site to the TBS, then diffuses from the TBS to the binding site below the site occupied

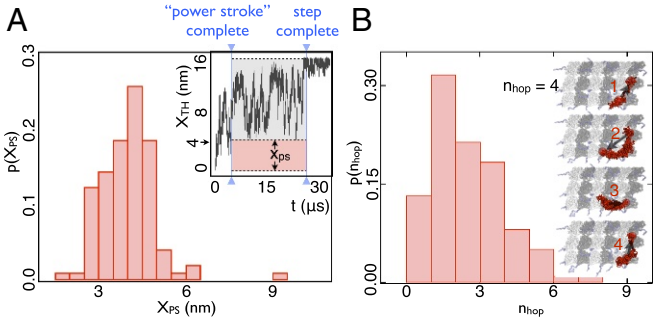

Fig. 3. Fraction of 16-nm step associated with power stroke. (*A*) Distribution of x_{ps}, the fraction of 16 nm associated with power stroke, based on 100 trajectories. *A*, *Inset* illustrates x_{ps} and also shows the time variation in the translational motion of x_{TH} the TH along the MT axis in a representative trajectory. The first vertical line (solid blue) shows the instant NL docking (power stroke) is complete, after which the TH undergoes diffusive motion. The top and middle horizontal lines (dotted blue lines) indicate the extent of diffusional search after NL docking. The distance between the top and middle line corresponds to the fraction associated with diffusion, while the distance between the middle and bottom line corresponds to the fraction associated with power stroke. (*B*) Distribution of n_{hop}, the number of hopping events (see text for definition) within the first 30 μs, based on 100 trajectories. Four hopping events in a single trajectory are illustrated on the right.

by the LH. Subsequently, the TH revisits the lower right binding site, before finally being captured by the TBS. On average, TH hops two to three times within 30 μs (Fig. 3*B*). The average hopping rate, calculated based on hundreds of such events, is $\sim 10\ \mu s^{-1}$.

The results in Fig. 3*B* suggest that the TH may hop multiple times during a single kinesin step, depending on the affinity between ADP-bound TH and the MT. If the affinity is sufficient to trap the ADP-bound TH at a specific binding site, which requires the correct orientation of the motor head (most likely the TBS) with respect to the MT, the TH may only hop between the geometrically allowed sites on the neighboring protofilaments one to three times within a step. On the other hand, if none of the accessible binding sites can trap the ADP-bound TH, hopping of the TH may persist until ADP release occurs. Release of ADP strengthens MT–Kin interaction and hence would result in the cessation of the diffusional search and stochastic hopping. Given that the ADP release time (∼10 ms) is much slower than the average hopping time between binding sites (∼10 μs), it is likely that TH could potentially hop hundreds of times within a single step.

NL Docking Constrains Diffusion of the TH to Minimize Side Steps. So far, we have provided four lines of evidence that support the diffusive nature of the kinesin step: (*i*) high-resolution recording of the translational and rotational motion of the TH (Fig. 2 *A*–*G*), (*ii*) multiple attempts to bind to the TBS (Fig. 2*H*), (*iii*) large diffusion length (Fig. 3*A*), and (*iv*) stochastic hopping between binding sites (Fig. 3*B*). These findings might give the erroneous impression that tethered diffusion alone could lead to a site 16 nm away on the same protofilament as the TBS, without NL docking playing a significant role. To explore if this is indeed the case, we perform a "mutation" simulation, in which NL docking is energetically unfavorable ($\epsilon_h^{LH-NL} = 0$). In this case, TH is more likely to visit binding sites on neighboring protofilaments besides the TBS (Fig. 4*A*). Just as in wild-type (WT) simulations (where docking is favorable), we find that the TH stochastically hops between the accessible binding sites due to the diffusive nature of head motion in the mutant simulations. However, in the absence of NL docking, the probability of TH hopping to binding sites on the neighboring protofilaments of the MT is

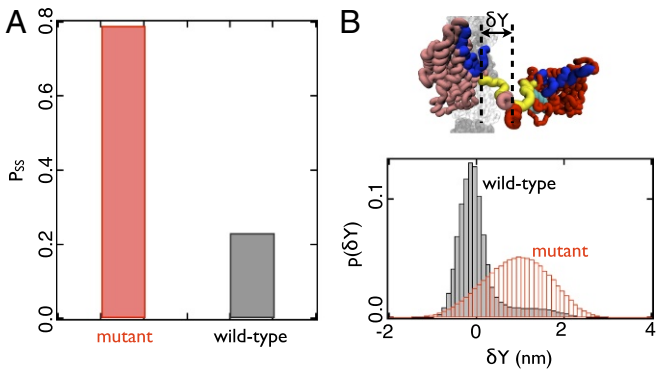

Fig. 4. NL docking decreases the probability of TH taking side steps. (*A*) Comparison of the probability of side steps in the mutant (docking is not energetically favorable) and WT (docking is energetically favorable) simulations. Here, $P_{ss} = \frac{\tau_{SBS}}{\tau_{TBS}+\tau_{SBS}+\tau_{IBS}}$. τ_{SBS} (τ_{TBS} and τ_{IBS}) is the average time the TH spends in the neighborhood of side binding sites on neighboring protofilaments (the TBS and IBS) over 100 trajectories. The TH is considered to be in the neighborhood if $d_{TH} < 4$ nm, where d is defined in the methods. (*B*) Distribution of sideway extension of LH–NL (δY) in the mutant and WT simulation, where $\delta Y = (\vec{r}_{LH}^{\,T338} - \vec{r}_{LH}^{\,T326}) \cdot \hat{e}^{y}$ with $\hat{e}^{y}$ being the unit vector along the y axis (Fig. 2).

much larger than the probability of reaching the TBS. In contrast, in the WT simulations, the probability of TH reaching the side and IBSs is substantially less than finding the TBS. The NL docking essentially prevents the tethered head from reaching the IBS, implying that, unlike in myosin V (36), rear foot stomping does not occur. Thus, the restriction imposed by NL docking facilitates kinesin to reach the TBS, even though the movement of the TH after detachment from MT is stochastic.

NL docking also decreases the probability of TH visiting side binding sites because it constrains the sideways extension of the LH NL. Our previous study (24) showed that, in order for the TH to take a side step, not only the TH NL, but also the LH NL needed to extend sideways. If docking is not energetically favorable, LH NL can extend sideways freely (red bins in Fig. 4*B*). However, the interaction between the catalytic core and the LH NL would limit the sideways extension of the LH NL if docking is energetically favorable (black bins in Fig. 4*B*). This, in turn, will reduce the diffusion coefficient somewhat (*SI Appendix*, Fig. S5) and decrease the distribution width of the TH along the y axis (Fig. 4*B*). Therefore, although NL docking contributes only 3–5 of 16 nm, it plays a crucial role in restricting the movement of kinesin on a single protofilament.

Dynamics of NL Docking and the Diffusing TH Are Uncorrelated. To illustrate how NL docking constrains the diffusion of the TH, we compare the displacement of the docking LH–NL and moving TH in a representative trajectory (*SI Appendix*, Fig. S2*A*). Specifically, we show the motion of T338 (*SI Appendix*, Fig. S2*B*, red) at the boundary between the coiled coil and the LH–NL (*SI Appendix*, Fig. S2*A*), which docks upon ATP binding. In the same figure, we also plot the motion of the center of mass of the TH (*SI Appendix*, Fig. S2*B*, black). Interestingly, the motion of the TH and the docking NL seems to be largely uncorrelated, except at the very early stages. At the instant when LH–NL reaches 5 nm (*SI Appendix*, Fig. S2*B*, first dot), the TH has already traveled a distance $\geq$10 nm, indicating that the diffusing TH is ahead of the docking LH–NL. *SI Appendix*, Fig. S2*B* shows a plateau in the dynamics of T338, during which x_{T338} does not change, while x_{TH} undergoes large changes. As x_{T338} fluctuates around 5 nm (*SI Appendix*, Fig. S2*B*, between the second and third dots), the x_{TH} diffuses between 4 and 12 nm. The only correlation between x_{T338} and x_{TH} seems to be that x_{T338} set a lower bound for x_{TH}, meaning x_{TH} rarely drops below the value of x_{T338} by more than $\sim$1 nm.

The lack of correlation between the time-dependent changes in x_{TH} and x_{T338} is more apparent in a plot x_{TH} as a function of x_{T338} (*SI Appendix*, Fig. S2*C*). The dotted line corresponds to $x_{TH} = x_{T338}$. Any data point above (below) the dotted line indicates that TH is ahead of (behind) the docking LH–NL. We find that TH follows LH–NL up to 3 nm, after which the TH is predominately ahead of the LH–NL. At the end of the step, the TH moves $\sim$16 nm, while LH–NL moves only $\sim$8 nm. Thus, given that the TH is ahead of the docking NL during the major duration of the step, it is inaccurate to suggest that TH is pulled by NL docking toward the (+) end of the MT. The TH reaches the TBS at the (+) end through diffusion, with NL docking providing the needed restriction and bias for the TH to reach the TBS.

NL Docking Is Not Necessary for Detachment of the TH from the MT. The mutation simulations also allow us to test the hypothesis that NL has to dock to release the TH from the MT. If this hypothesis is correct, we expect that the TH would stay bound to the MT in the mutation simulations (Fig. 5*B*). However, TH detaches from the MT (Fig. 5*A*) within 5 μs (Fig. 5*C*) in 79% of trajectories. Thus, the intramolecular strain within a two-head-bound state alone is sufficient to detach the TH. When the intramolecular strain is released by deleting the LH, the TH stays bound to the MT within our simulation window (50 μs) and can resist external force up to 3 pN. Therefore, NL docking in the LH is not necessary to release the ADP-bound TH from the MT.

Our observation is not inconsistent with the LH gating model (37, 38). According to the model, ATP cannot bind to the LH until the TH detaches from the MT. In other words, intramolecular stain in the two-head-bound state inhibits ATP binding and thus NL docking to the LH. Therefore, the LH gating model predicts that TH detachment from the MT occurs before NL docking to the LH. This prediction is supported by our finding that TH detachment from the MT does not depend on docking of NL to the LH.

Discussion

We use simulations of a CG model with hydrodynamic interactions (HIs) of the entire MT–Kin complex to (*i*) quantify the contribution of NL docking and diffusion to the kinesin step and (*ii*) illustrate the mechanism by which kinesin avoids side steps. Our model, which is currently the only one to include the effects of MT explicitly, is calibrated to reproduce the experimentally measured stall force (10, 11, 39) and the force required to

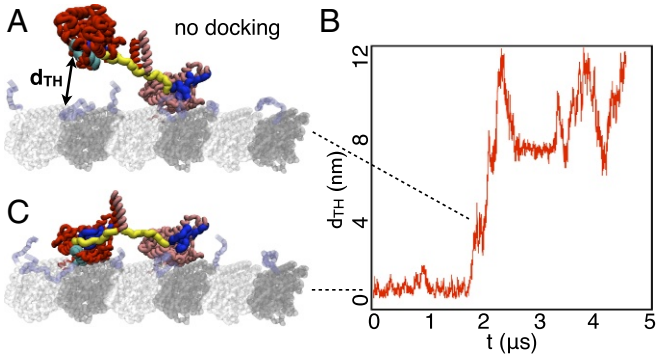

Fig. 5. NL docking is not necessary to detach to the TH from the MT. (*A*) A snapshot showing TH detaches from the MT, while the NL of the LH remains undocked. (*B*) The initial conformation of the kinesin motor heads in the mutant simulation, where NL docking does not occur. (*C*) The distance between the TH and the MT as a function of time recorded in the mutant simulation.

dislodge the motor head from the MT (31, 40) (*SI Appendix*, Fig. S1). Interestingly, these two energy scales suffice to capture all of the salient features of the kinesin step. Surprisingly, we find that nearly three-quarters of the 16-nm step involves an almost random search for the TBS by the TH (Figs. 1 and 3). The time the TH spends in the stochastic search accounts for >95% of the duration for completing the 16-nm step (Fig. 1*E*). However, to stay predominantly on the same protofilament of the MT, NL docking is necessary to constrain the diffusion of the TH, thus minimizing the probability of side steps (Fig. 4).

Our simulations underscore the importance of large-scale diffusive motion within the kinesin step (Fig. 1). One might argue that the stochasticity observed in the simulation is due to the simplicity of the self-organized polymer (SOP) model, which is based on short-ranged native contacts. The SOP model allows for fluctuations in the NL, before it becomes fully docked to the LH. So, could a simulation, where NL docking in the LH is triggered by less flexible Go-like model, produce a 16-nm step with decreased stochasticity? It is unlikely for two reasons. First, even assuming that the LH NL docks deterministically, TH NL, which is undocked and connects TH and LH, would introduce stochasticity due to the translation of the TH. At the same time, TH is free to rotate, regardless of the conformational state of the LH NL. Second, temporally NL docking accounts for <5% of the stepping time. Spatially, NL docking could pull TH toward the (+) end by 8 nm at most. The rest of the step has to occur through diffusion, which is independent of the dynamics of NL docking. It is also worth noting that HO have shown that the SOP model and the one including dihedral angle potentials in the Go-like model lead to qualitatively similar equilibrium properties, further justifying our used of the SOP model (supporting information in ref. 23). Thus, the physics of kinesin stepping illustrated here is not dependent on the apparent increase in the flexibility of the model.

It is difficult to capture the bidirectional motion of the kinesin motor domain by using only the current experimental techniques, due to the small size of the kinesin motor domain (41) (~2 nm) and the transient nature of the 16-nm step (11) (~30 μs). From a theoretical perspective, however, it seems natural to suggest that diffusion must play a key role in kinesin motility. The rate of diffusion (~4 μs^{-1}, for 16 nm) is much faster than the rate of ATP turnover (~1 ms^{-1}). To experimentally test our prediction of the extent (~12 nm) and duration (~40 μs) of diffusion within the kinesin step, would require tracking the motion of the kinesin motor head by using optical trap (42) or FIONA (5) at approximately microsecond resolution.

In a recent experiment (22), the motion of the unbound head was tracked at high temporal (≈ 55 μs) resolution by using dark-field microscopy. By tracking the position of a 40-nm gold particle connected to the motor head through a biotin–streptavidin construct, it was shown that the motion of the unbound head toward the TBS occurs by diffusion, in accord with our previous findings (24). The large hydrodynamic drag due to the gold particle slows down the actual time scale for stepping, suggesting that the extent of diffusion could be even greater than hinted at by these insightful experiments. Even with this high temporal resolution, subtle aspects of search for the TBS, such as nearly unhindered rotation of the unbound head and multiple attempts to achieve correct orientation of the motor head with respect to the MT, as discovered here, will have to await future experiments involving labeling at multiple sites and higher temporal resolution.

The observation that NL docking is responsible for only ~4 nm of the 16-nm step (Fig. 3*A*) shows that NL docking cannot directly pull the motor head to the next binding site. In this respect, NL docking in kinesin is different from lever arm rotation in myosin. This difference is also supported by experiments (28, 43). If a step is largely due to the conformational change in a mechanical motif (such as docking of the NL or rotation of the lever arm) of a motor protein, then extension of the mechanical motif should lead to an increase of step size and motor speed. Indeed, the sliding velocity of the myosin motor increases linearly with the length of its lever arm (44). In contrast, extending the NL by stiff helices or double-stranded DNA does not lead to any increase of kinesin speed (28, 43). Therefore, NL docking and lever arm rotation must contribute to motor motility in different ways.

The finding that NL docking in the LH is not necessary for detachment of the TH (Fig. 5) is consistent with experiments (38, 45). Using single-molecule FRET, Mori et al. showed that at low ATP concentrations, kinesin waits in a one-head-bound state (45). Given that NL docking is triggered by ATP binding, this result suggests that the TH can detach spontaneously in the absence of NL docking. Further, using fluorescence polarization microscopy, Asenjo and Sosa provided evidence that the TH is mobile while kinesin waits for ATP (46). Our findings support a recent experiment demonstrating that intramolecular strain generated by NL docking is not necessary to accelerate the detachment of the TH (38). According to our simulations, intramolecular strain generated by the two-head-bound state alone could cause the detachment of the TH within 5 μs in most instances.

From our study, we infer a physically reasonable mechanism for avoiding side steps: NL docking limits the access to side binding sites and prevents rebinding to the initial site by constraining TH diffusion (Figs. 4 and 6). Such a mechanism has been proposed earlier in an important computational study (23) and simulation from our group (24). Using a computational model based on the potential of mean force experienced by the TH, HO found that the probability of TH taking side steps depends on the rate of NL docking to the LH (23). In accord with this finding based on equilibrium simulations, we show, using detailed stepping dynamics, that NL docking reduces the probability of side steps (24). In the present study, we calibrate the energy scales associated with docking, by reproducing experimentally measured stall force. We find that docking occurs fast within 1.1 μs, which is <20 μs, the maximum docking time, estimated from

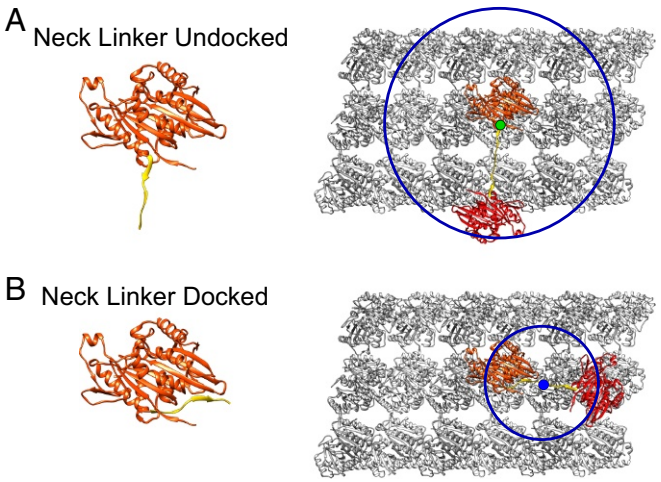

Fig. 6. A model for how kinesin chooses its binding site. Schematics of binding sites accessible to the TH in the absence (*A*) and presence (*B*) of NL docking are shown. The circles illustrate the range of sites that are accessible to a free motor head. In *A*, the blue sites can be reached with significant probability if NL docking is disfavored. Upon NL docking to the LH, the most probable site to which the TH binds is the one that is along the same protofilament. In both cases, the search for various binding sites occurs by stochastic movement after the TH detaches from the MT.

the equilibrium simulations (23), to avoid side steps. Therefore, despite differences in the simulation strategies, both studies show that NL docking reduces the probability of side steps.

However, could side steps be avoided by other mechanisms? For example, instead of limiting the access to side binding sites (Fig. 6*B*), is it possible to prevent ADP release at these sites (sites within the blue circle in Fig. 6*A*)? Preferential ADP release is supported by previous experiments. ADP–kinesin affinity is lower when NL points toward the minus end of the MT (31, 40), implying that the TH is more likely to release the bound ADP when it closer to the TBS than the IBS. However, the observation that the probability of side steps is >50% for a kinesin mutant with extended NL (28) suggests that TH can release ADP at accessible binding sites (blue dots in Fig. 6*A*) other than the TBS. Therefore, to minimize the probability of taking side steps, it is necessary to limit the access of the TH to side binding sites by constraining TH diffusion (Fig. 6*B*). One simple and elegant way that nature has solved this problem is by constraining the walk through NL docking.

Conclusions

Our results unify two seemingly distinct mechanisms in kinesin stepping, the NL docking model (8) and the Brownian ratchet model (18). Furthermore, we also provide a structural explanation for how kinesin stays on a single MT protofilament. Our simulations show that kinesin takes the 16-nm step mainly through Brownian motion, with NL docking crucially constraining the Brownian motion of the kinesin motor head.

Materials and Methods

We perform simulations by creating a CG model of the MT–Kin complex (details in *SI Appendix*). Such models have proved to be efficacious in producing quantitative insights into the stepping kinetics of molecular motors (23, 30, 47–50). Additional details, including the creation of the MT–Kin complex with coiled coil and cargo based on the SOP model (51–53), the determination of the two important parameters, and the simulation details are given in the *SI Appendix*. Remarkably, only two parameters are needed to quantitatively describe the stepping kinetics, with one accounting for the strength of the NL attachment to the LH and the other being the strength of the motor head-MT interaction.

We use Brownian dynamics with HIs to generate a large ensemble of stepping trajectories. It is important to point out that to observe completion of steps in an experimentally relevant time scale, HIs must be explicitly included (54). Finally, we note that the use of CG model allows us to generate hundreds of trajectories for both the WT and in silico mutants, created by assigning zero gain in the energy due to ordering of the NL to the LH, so that conclusions with sufficient statistics can be drawn.

ACKNOWLEDGMENTS. We thank Dr. K. H. Downing for providing the coordinates of MT; Prof. Michael E. Fisher for interactions during the course of this work, which was done as a partial fulfillment of the doctoral thesis (Z.Z.) requirement in 2012; and Mauro Mugnai and Naoto Hori for constructive suggestions. This work was supported by National Science Foundation Grant CHE 16-61946. Additional support was provided by Collie-Welch Reagents Chair F-0019.

1. Howard J (2001) *Mechanics of Motor Proteins and the Cytoskeleton* (Sinauer Associates, Sunderland, MA).
2. Vale RD (2003) The molecular motor toolbox for intracellular transport. *Cell* 112:467–480.
3. Block SM (2007) Kinesin motor mechanics: Binding, stepping, tracking, gating, and limping. *Biophys J* 92:2986–2995.
4. Hancock WO (2016) The kinesin-1 chemomechanical cycle: Stepping toward a consensus. *Biophys J* 110:1216–1225.
5. Yildiz A, Tomishige M, Vale RD, Selvin PR (2004) Kinesin walks hand-over-hand. *Science* 303:676–678.
6. Asbury CL, Fehr AN, Block SM (2003) Kinesin moves by an asymmetric hand-over-hand mechanism. *Science* 302:2130–2134.
7. Hua W, Chung J, Gelles J (2002) Distinguishing inchworm and hand-over-hand processive kinesin movement by neck rotation measurements. *Science* 295:844–848.
8. Rice S, et al. (1999) A structural change in the kinesin motor protein that drives motility. *Nature* 402:778–784.
9. Schnitzer M, Block S (1997) Kinesin hydrolyses one ATP per 8-nm step. *Nature* 388:386–390.
10. Svoboda K, Block S (1994) Force and velocity measured for single kinesin molecules. *Cell* 77:773–784.
11. Carter NJ, Cross RA (2005) Mechanics of the kinesin step. *Nature* 435:308–312.
12. Spudich JA, Sivaramakrishnan S (2010) Myosin VI: An innovative motor that challenged the swinging lever arm hypothesis. *Nat Rev Mol Cell Biol* 11:128–137.
13. Gennerich A, Carter AP, Reck-Peterson SL, Vale RD (2007) Force-induced bidirectional stepping of cytoplasmic dynein. *Cell* 131:952–965.
14. Reck-Peterson SL, et al. (2006) Single-molecule analysis of dynein processivity and stepping behavior. *Cell* 126:335–348.
15. Gennerich A, Vale RD (2009) Walking the walk: How kinesin and dynein coordinate their steps. *Curr Opin Cell Biol* 21:59–67.
16. Schief WR, Howard J (2001) Conformational changes during kinesin motility. *Curr Opin Cell Biol* 13:19–28.
17. Carter NJ, Cross RA (2006) Kinesin's moonwalk. *Curr Opin Cell Biol* 18:61–67.
18. Taniguchi Y, Nishiyama M, Ishii Y, Yanagida T (2005) Entropy rectifies the Brownian steps of kinesin. *Nat Chem Biol* 1:342–347.
19. Tomishige M, Stuurman N, Vale RD (2006) Single-molecule observations of neck linker conformational changes in the kinesin motor protein. *Nat Struct Mol Biol* 13:887–894.
20. Asenjo AB, Weinberg Y, Sosa H (2006) Nucleotide binding and hydrolysis induces a disorder-order transition in the kinesin neck-linker region. *Nat Struct Mol Biol* 13:648–654.
21. Khalil AS, et al. (2008) Kinesin's cover-neck bundle folds forward to generate force. *Proc Nat Acad Sci USA* 105:19247–19252.
22. Isojima H, Lino R, Aiitani Y, Noji H, Tomishige M (2016) Direct observation of intermediate states during the stepping motion of kinesin-1. *Nat Chem Biol* 12:290–297.
23. Hyeon C, Onuchic JN (2007) Mechanical control of the directional stepping dynamics of the kinesin motor. *Proc Natl Acad Sci USA* 104:17382–17387.
24. Zhang Z, Thirumalai D (2012) Dissecting the kinematics of the kinesin step. *Structure* 20:628–640.
25. Kutys ML, Fricks J, Hancock WO (2010) Monte Carlo analysis of neck linker extension in kinesin molecular motors. *PLoS Comput Biol* 6(11):e1000980.
26. Ray S, Meyhofer E, Milligan RA, Howard J (1993) Kinesin follows the microtubules protofilament axis. *J Cell Biol* 121:1083–1093.
27. Block SM, Asbury CL, Shaevitz JW, Lang MJ (2003) Probing the kinesin reaction cycle with a 2D optical force clamp. *Proc Natl Acad Sci USA* 100:2351–2356.
28. Yildiz A, Tomishige M, Gennerich A, Vale RD (2008) Intramolecular strain coordinates kinesin stepping behavior along microtubules. *Cell* 134:1030–1041.
29. Svoboda K, Schmidt CF, Schnapp BJ, Block SM (1993) Direct observation of kinesin stepping by optical trapping interferometry. *Nature* 365:721–727.
30. Hyeon C, Thirumalai D (2011) Capturing the essence of folding and functions of biomolecules using coarse-grained models. *Nat Commun* 2:487.
31. Uemura S, et al. (2002) Kinesin-microtubule binding depends on both nucleotide state and loading direction. *Proc Natl Acad Sci USA* 99:5977–5981.
32. Woehlke G, et al. (1997) Microtubule interaction site of the kinesin motor. *Cell* 90:207–216.
33. Nitta R, Okada Y, Hirokawa N (2008) Structural model for strain-dependent microtubule activation of Mg-ADP release from kinesin. *Nat Struct Mol Biol* 15:1067–1075.
34. Hinczewski M, Tehver R, Thirumalai D (2013) Design principles governing the motility of myosin V. *Proc Natl Acad Sci USA* 110:E4059–E4068.
35. Purcell T, Morris C, Spudich J, Sweeney H (2002) Role of the lever arm in the processive stepping of myosin V. *Proc Natl Acad Sci USA* 99:14159–14164.
36. Kodera N, Yamamoto D, Ishikawa R, Ando T (2010) Video imaging of walking myosin V by high-speed atomic force microscopy. *Nature* 468:72–77.
37. Guydosh N, Block S (2006) Backsteps induced by nucleotide analogs suggest the front head of kinesin is gated by strain. *Proc Natl Acad Sci USA* 103:8054–8059.
38. Andreasson JOL, et al. (2015) Examining kinesin processivity within a general gating framework. *Elife* 4:e07403.
39. Visscher K, Schnitzer M, Block S (1999) Single kinesin molecules studied with a molecular force clamp. *Nature* 400:184–189.
40. Uemura S, Ishiwata S (2003) Loading direction regulates the affinity of ADP for kinesin. *Nat Struct Biol* 10:308–311.
41. Kull F, Sablin E, Lau R, Fletterick R, Vale R (1996) Crystal structure of the kinesin motor domain reveals a structural similarity to myosin. *Nature* 380:550–555.
42. Guydosh NR, Block SM (2009) Direct observation of the binding state of the kinesin head to the microtubule. *Nature* 461:125–128.
43. Miyazono Y, Hayashi M, Karagiannis P, Harada Y, Tadakuma H (2010) Strain through the neck linker ensures processive runs: A DNA-kinesin hybrid nanomachine study. *EMBO J* 29:93–106.
44. Uyeda T, Abramson P, Spudich J (1996) The neck region of the myosin motor domain acts as a lever arm to generate movement. *Proc Natl Acad Sci USA* 93:4459–4464.
45. Mori T, Vale RD, Tomishige M (2007) How kinesin waits between steps. *Nature* 450:750–754.
46. Asenjo AB, Sosa H (2009) A mobile kinesin-head intermediate during the ATP-waiting state. *Proc Natl Acad Sci USA* 106:5657–5662.
47. Hyeon C, Onuchic JN (2007) Internal strain regulates the nucleotide binding site of the kinesin leading head. *Proc Natl Acad Sci USA* 104:2175–2180.
48. Hwang W, Lang MJ, Karplus M (2008) Force generation in kinesin hinges on cover-neck bundle formation. *Structure* 16:62–71.
49. Hariharan V, Hancock WO (2009) Insights into the mechanical properties of the kinesin neck linker domain from sequence analysis and molecular dynamics simulations. *Cell Mol Bioeng* 2:177–189.

50. Grant BJ, et al. (2011) Electrostatically biased binding of kinesin to microtubules. *PLoS Biol* 9:e1001207.
51. Hyeon C, Dima RI, Thirumalai D (2006) Pathways and kinetic barriers in mechanical unfolding and refolding of RNA and proteins. *Structure* 14:1633–1645.
52. Hyeon C, Lorimer GH, Thirumalai D (2006) Dynamics of allosteric transitions in GroEL. *Proc Natl Acad Sci USA* 103:18939–18944.
53. Chen J, Dima RI, Thirumalai D (2007) Allosteric communication in dihydrofolate reductase: Signaling network and pathways for closed to occluded transition and back. *J Mol Biol* 374:250–266.
54. Goldtzvik Y, Zhang Z, Thirumalai D (2016) Importance of hydrodynamic interactions in the stepping kinetics of kinesin. *J Phys Chem B* 120:2071–2075.